A New High Efficiency and Low Profile On-Board DC/DC Converter for Digital Car Audio Amplifier

Chong-Eun Kim, Sang-Kyoo Han, Gun-Woo Moon

Department of Electrical Engineering and Computer Science,
Korea Advanced Institute of Science and Technology, Daejeon, Korea
Email: gwmoon@ee.kaist.ac.kr

Abstract: A new high efficiency and low profile on-board DC/DC converter for digital car audio amplifier is proposed. The proposed converter shows the continuous input current, no DC excitation current of the transformer, the minimized electro-magnetic interference (EMI), no output inductor, and the low voltage stress of the secondary rectifier diodes. The 60W industrial sample of the proposed converter is implemented for digital car audio amplifier and the measured efficiency is 88.3% at nominal input voltage.

1. Introduction

Generally, the analog audio amplifier has excellent distortion characteristics, but shows the considerably low efficiency and needs the bulky heat sinks for cooling. On the other hand, the digital audio amplifier has the high efficiency and the compact size, but the relatively poor fidelity. Nowadays, since the digital audio amplifier technology is developed and its fidelity characteristics are improved as reported in [1], it is applied to the compact car audio system.

Therefore, the high efficiency and low profile on-board DC/DC converter is required for digital car audio amplifiers. Among the previously proposed DC/DC converters, the boost integrated half bridge (BHB) converter shown in Fig. 1 is suitable for low voltage battery input applications, because the converter has the continuous input current, I_{LIN}, and the boosted link voltage, V_L. In addition, the primary MOSFETs are turned-on in zero-voltage-switching (ZVS) condition [2-3]. However, the main disadvantages of the BHB converter are the high DC excitation current of the transformer, the high voltage stress and the large turn-off voltage oscillation of the secondary rectifier diodes, the increased magnetic components count, and the considerable freewheeling energy in the transformer.

In this paper, to overcome these disadvantages of the BHB converter, a new high efficiency and low profile on-board DC/DC converter is proposed. The operational principles of the proposed converter are analyzed and the advantages are described. The 60W industrial sample for digital car audio amplifier is implemented to verify the operational principles and advantages of the proposed converter.

2. Principles of Operation

As shown in Fig. 2, the proposed converter is the asymmetrically controlled half bridge converter integrated with the boost converter as the front stage and with the rectifier stage of the voltage doubler type.

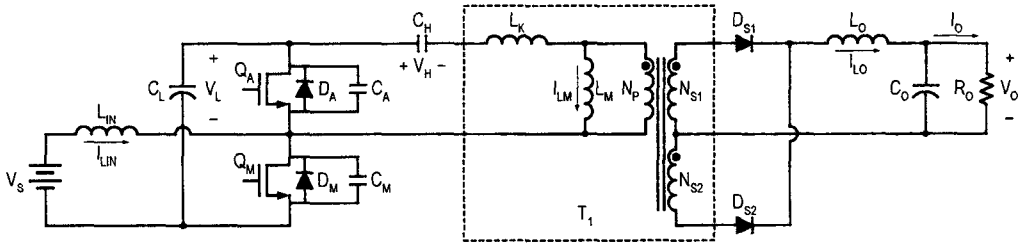

Fig. 1. Conventional BHB converter

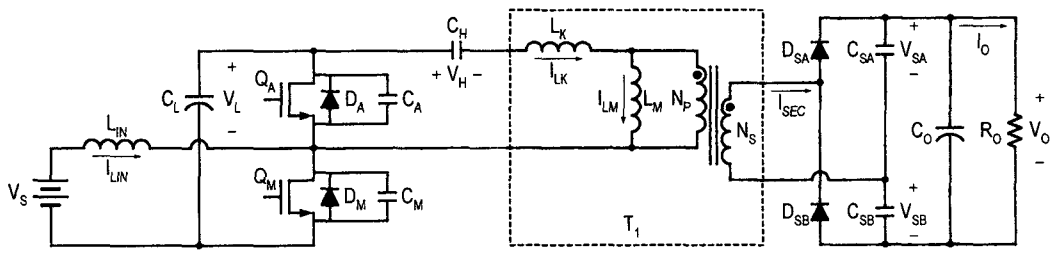

Fig. 2. Circuit diagram of the proposed converter

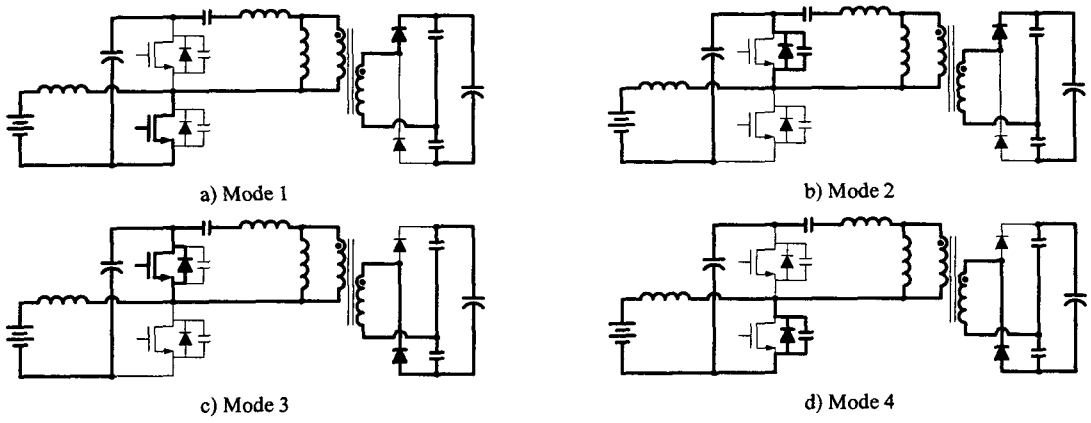

Fig. 3. Operational modes of the proposed converter

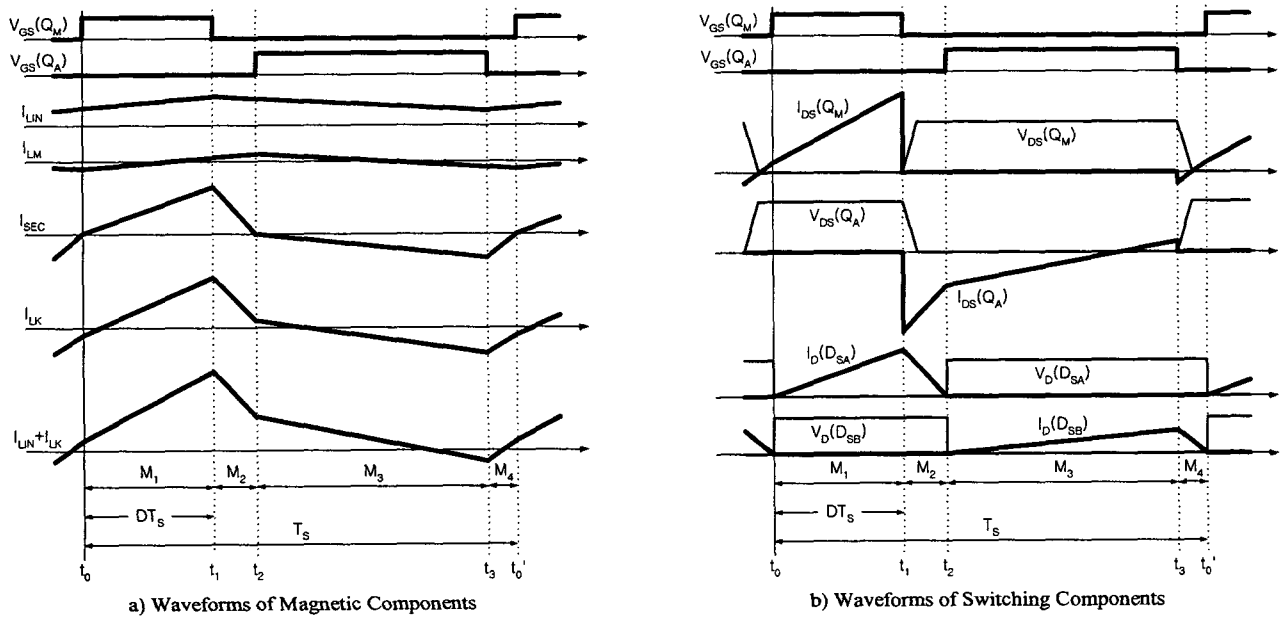

a) Waveforms of Magnetic Components

b) Waveforms of Switching Components

Fig. 4. Key waveforms of the proposed converter

2.1 Mode Analysis

The proposed converter operates in four modes according to the switching states of the primary MOSFETs and the secondary diodes. The operational modes and the key waveforms are presented in Fig. 3 and Fig. 4, respectively.

Mode 1 (M_1, t_0~t_1): When Q_M is turned-on at t_0, mode 1 begins as shown in Fig. 3 a). The boost inductor current, I_{LIN}, and the transformer primary current, I_{LK}, flow through Q_M, and they are increased by V_S and $[(V_L-V_H)-(N_P/N_S)V_{SA}]$, respectively. The transformer secondary current, I_{SEC}, is linearly increased flowing through D_{SA}, while C_{SA} is charged and C_{SB} is discharged.

Mode 2 (M_2, t_1~t_2): When Q_M is turned-off, mode 2 begins at t_1 as shown in Fig. 3 b). I_{LIN} and I_{LK} flow through the body diode of Q_A. Since the value of V_L is greater than that of V_S in steady-state, I_{LIN} is steeply decreased with the current slope of $(V_S-V_L)/L_{IN}$. I_{LK} is also linearly decreased with the current slope of $[(-V_H)-(N_P/N_S)V_{SA}]/L_K$. I_{SEC} flows through D_{SA} and linearly decreases, while C_{SA} is charged and C_{SB} is discharged.

Mode 3 (M_3, t_2~t_3): When the commutation of the secondary diodes currents is completed, i.e. D_{SA} is turned-off and D_{SB} is conducting, mode 3 begins at t_2 as shown in Fig. 3 c). As the same of mode 2, I_{LIN} still flows to DC link capacitor, C_L, with the current slope of $(V_S-V_L)/L_{IN}$ through the body diode of Q_A. I_{LK} flows through Q_A, and is decreased with the current slope of $[(-V_H)+(N_P/N_S)V_{SB}]/L_K$. I_{SEC} flows through D_{SB} and linearly decreases, while C_{SA} is discharged and C_{SB} is charged.

Mode 4 (M_4, t_3~t_0'): When Q_A is turned-off at t_3, mode 4 begins as shown in Fig. 3 d). I_{LIN} flows through Q_M with the current slope of V_S/L_{IN}. After the voltage across C_M is decreased to 0V, I_{LK} flows through the body diode of Q_M. In addition, I_{LK} is linearly increased with the current slope of $[(V_L-V_H)+(N_P/N_S)V_{SB}]/L_K$. I_{SEC} flows through D_{SB} and linearly decreases, while C_{SA} is discharged and C_{SB} is charged.

2.2 Input-Output Voltage Conversion Ratio

In order to derive the output voltage equation, it is assumed that V_L, V_H, V_{SA}, V_{SB}, and V_O are constant during the switching period. Since the time intervals of mode 2 and mode 4 are much smaller than the switching period, these modes can be disregarded for the simplicity of the analysis. By applying the voltage·second product equations on L_{IN}, L_K, and L_M during one switching period, the following equations can be easily obtained.

$$V_L = \frac{1}{1-D} V_S \tag{1}$$

$$V_H = \frac{D}{1-D} V_S \tag{2}$$

$$V_{SA} = (1-D) V_O \tag{3}$$

$$V_{SB} = D V_O \tag{4}$$

where D is the duty ratio of Q_M. Since the output load current equals to the half of the average value of the absolute transformer secondary current, it is given by

$$I_O = \frac{1}{4F_S} \frac{N_P}{N_S} \left[\frac{V_L}{L_K} - \left(\frac{1}{L_K} + \frac{1}{L_M} \right) \frac{N_P}{N_S} V_O \right] D(1-D), \tag{5}$$

where F_S is the switching frequency. By substituting the equations (1), (2), (3), and (4) for (5), the input-output voltage conversion ratio can be obtained as follows.

$$\frac{V_O}{V_S} = \frac{\frac{N_S}{N_P} D}{\frac{4L_K F_S}{R_O} \left(\frac{N_S}{N_P} \right)^2 + \left(1 + \frac{L_K}{L_M} \right) D(1-D)} \tag{6}$$

The input-output voltage conversion ratio is plotted as a function of the duty ratio D in Fig. 5 in the condition of $N_P/N_S = 1$, $L_M = 100\mu H$, $L_K = 2\mu H$, $F_S = 100kHz$, and $R_O = 12\Omega$.

2.3 Advantages of Proposed Converter

The advantages of the proposed converter are as follows:

i) The BHB converter has DC offset of the transformer magnetizing current given by

$$DC\ Excitation\ Current = I_{L_M,DC} = \frac{N_S}{N_P}(1-2D)\frac{V_O}{R_O}, \tag{7}$$

where $N_S = N_{S1} = N_{S2}$. On the other hand, the proposed converter has no DC offset of the transformer magnetizing current due to the series-connected DC blocking capacitors, C_H, C_{SA}, and C_{SB}. As a result, since the optimal flux design of the transformer core is possible, the size of the transformer can be minimized or heat of the transformer can be greatly reduced.

ii) The voltage stress of secondary diodes, D_{S1} and D_{S2}, in the BHB converter is given by

$$Voltage\ Stress\ of\ D_{S1} = V_{D_{S1}} = 2\frac{N_S}{N_P} V_H = V_O/(1-D), \tag{8}$$

$$Voltage\ Stress\ of\ D_{S2} = V_{D_{S2}} = 2\frac{N_S}{N_P}(V_L - V_H) = V_O/D, \tag{9}$$

where $N_S = N_{S1} = N_{S2}$. Therefore, the voltage stress of D_{S2} increases at the high input voltage and light load condition. On the other hand, in the proposed converter, the voltage stresses of the secondary rectifier diodes, D_{SA} and D_{SB}, are always clamped to the output voltage V_O regardless of the duty ratio D as follows.

$$Voltage\ Stress\ of\ D_{SA} = V_{D_{SA}} = V_O \tag{10}$$

$$Voltage\ Stress\ of\ D_{SB} = V_{D_{SB}} = V_O \tag{11}$$

The voltage stresses, normalized by V_O, of the secondary diodes in both converters as functions of the duty ratio D are shown in Fig. 6.

iii) In the conventional BHB converter, the serious voltage ringing exist in the secondary diodes. Thus, RC snubber or transient-voltage-suppressor (TVS) has to be used, which deteriorated the efficiency. On the other hand, since the secondary diodes of the proposed converter are turned-off in zero-current-switching (ZCS) condition, the turn-off voltage oscillation is very small. Therefore, since there is no necessity for use of the snubbers, the high efficiency of the proposed converter can be obtained.

iv) Since the proposed converter has no output inductor, the reduced conduction loss can be obtained, and desirable for low cost.

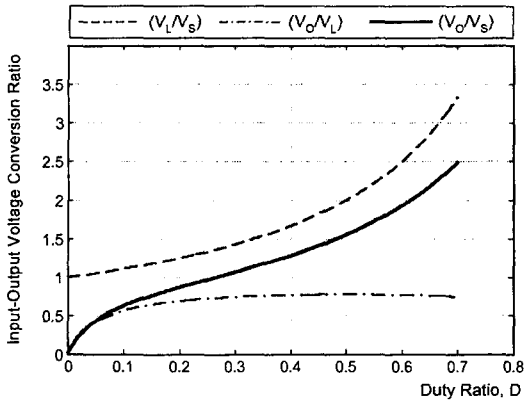

Fig. 5. Input-output voltage conversion ratio

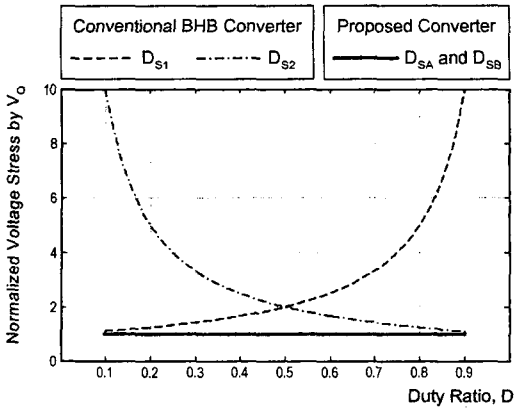

Fig. 6. Normalized voltage stress of the secondary diodes

v) In the BHB converter, the non-power-transfer time interval exits due to the commutation of D_{S1} and D_{S2}. Thus, the effective duty ratio, D_{eff}, is decreased in the BHB converter as the following equation.

$$D_{eff} = D - 2L_K I_{L_o} F_S \frac{N_S}{N_P}\left(\frac{1}{V_H} + \frac{1}{V_L - V_H}\right) \quad (12)$$

On the other hand, the proposed converter always transfers the power of the primary stage to the secondary stage in the overall switching period and has no freewheeling energy. Thus, the high efficiency can be obtained without large circulating energy losses in the proposed converter.

vi) Since the primary MOSFETs, Q_M and Q_A, of the proposed converter are turned-on in ZVS condition, the switching loss can be minimized.

vii) Since the input current is continuous, the proposed converter has the minimized input filter.

Although the current stresses of the secondary diodes in the proposed converter are rather large compared with that in the conventional BHB converter, the proposed converter has the high efficiency due to the minimized conduction and switching losses. Furthermore, the proposed converter shows the desirable features such as high power density and low profile due to the reduced count and size of magnetic components. In addition, the proposed converter has the low EMI due to the wide ZVS range of the primary MOSFETs, and ZCS turn-off of the secondary diodes.

3. Experimental Results

To verify the operational principles and the feasibility of the proposed converter, the 60W industrial sample of the proposed converter is implemented by employing the metal printed-circuit-board (PCB) for digital car audio amplifier. The circuit diagram and control scheme of the proposed system are shown in Fig. 7 and Fig. 8, respectively. As can be seen in Fig. 7, the proposed converter produces ± 18V and ± 8V for power supply of power stage and controller of the digital car audio amplifier, respectively. The dimension of the industrial sample is 129(L)x48(W)x13(H) [mm] and its photograph is presented in Fig. 9.

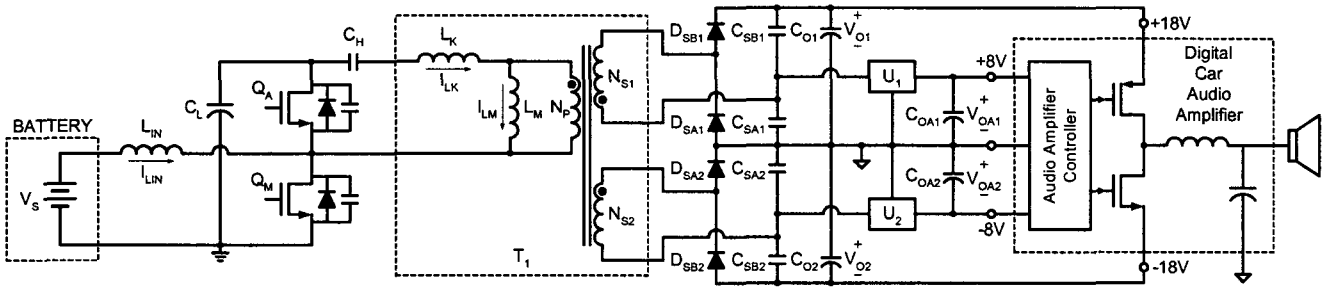

Fig. 7. Circuit diagram of 60W sample for digital car audio amplifier

The design specifications of the sample are shown in Table 1, and the circuit parameters and components are selected as Table 2. The input current is continuous and its waveform at nominal input voltage is shown in Fig. 10. Fig. 11 shows the transformer primary current, I_{LK}. Fig. 12 shows the output voltages of +18V and –18V with greatly reduced output voltage ripples. The switching waveforms of the proposed converter at minimum and maximum input voltages are presented in Fig. 13 and Fig. 14, respectively.

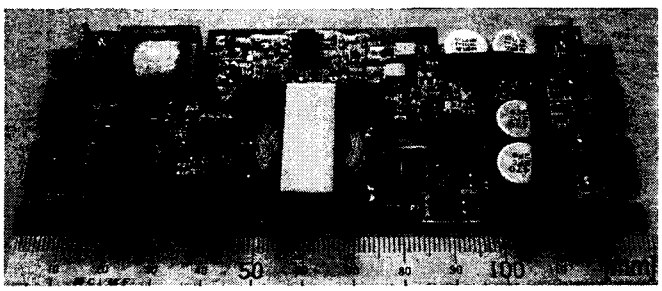

Fig. 9. Photograph of 60W sample for digital car audio amplifier

Table 1. Design Specification for Digital Audio Amplifier

Input Voltage, V_S	10V ~ 16V, 12V Nominal
Output Voltage, V_O	+18V(1.5A) and –18V(1.5A)
Auxiliary Output Voltage, V_{OA}	+8V(0.4A) and –8V(0.4A)
Maximum Output Power, $P_{O,max}$	60W
Switching Frequency, F_S	100kHz

Table 2. Circuit Parameters for Digital Audio Amplifier

L_{IN}	50μH, EPC17 (TDK)
C_L	100μF, 35V, Electrolytic, 2EA
C_H	22μF, 25V, MLCC, 2EA
C_{SA1}, C_{SB1}, C_{SA2}, C_{SB2}	22uF, 25V, MLCC
	22uF, 25V, Tantal
C_{O1}, C_{O2}	470uF, 35V, Electrolytic, 2EA
COA1, COA2	10uF,16V, MLCC
T_1	PQ2610 (Magnetics)
	L_M = 100μH, L_K = 2μH
	N_P = 3, N_{S1} = 3, N_{S2} = 3
Q_M	IRF1104S, D2-Pak
Q_A	IRFR3504, D-Pak
D_{SA1}, D_{SB1}, D_{SA2}, D_{SB2}	12CWQ03FN, D-Pak
U_1	UA78M08C, D-Pak
U_2	UA79M08C, D-Pak

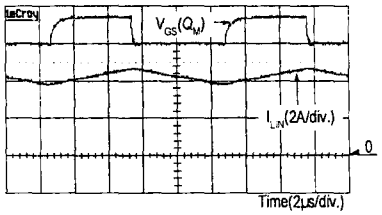

Fig. 10. Waveform of I_{LIN}

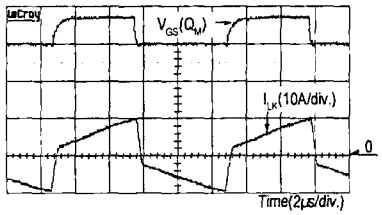

Fig. 11. Waveforms of I_{LK}

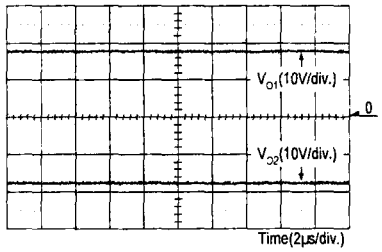

Fig. 12. Waveforms of output voltages

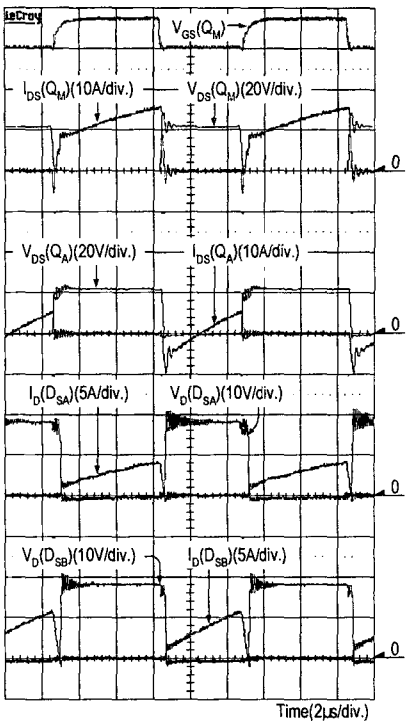

Fig. 13. Waveforms of switching components at V_S = 10V

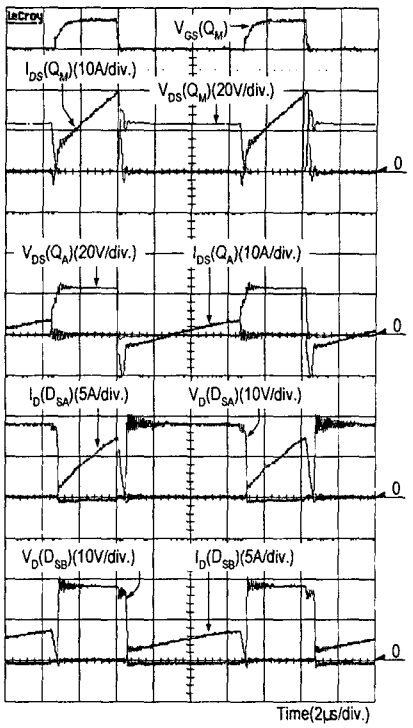

Fig. 14. Waveforms of switching components at V_S = 16V

As can be seen in these figures, the switches, Q_M and Q_A are turned-on in the ZVS condition and the secondary rectifier diodes are turned-off in ZCS condition. In addition, the voltage stress of the secondary rectifier diodes is clamped to the output voltage and the voltage oscillation is considerably small without the snubbers. The measured efficiencies of the proposed converter and the BHB converter are compared in Fig. 15. At nominal input voltage, the efficiency of the proposed converter is 88.3% and that of the BHB converter 84.8%. As can be seen in Fig. 15, the proposed converter shows higher efficiency than the conventional BHB converter.

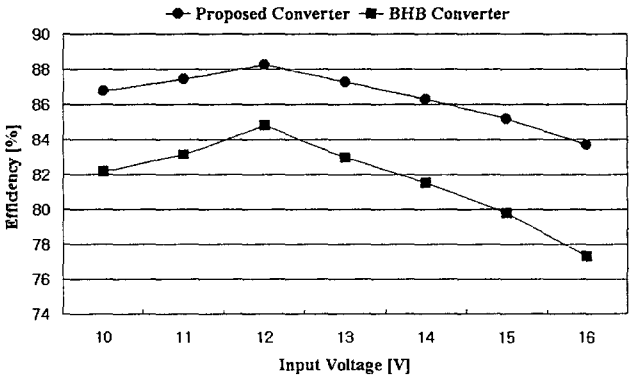

Fig. 15. Measured efficiencies

4. Conclusion

In this paper, a new high efficiency and low profile on-board DC/DC converter for digital car audio amplifier is proposed. The proposed converter shows no DC excitation current of transformer, the low voltage stress and ZCS turn-off of the secondary diodes, and no output inductor. Furthermore, the proposed converter shows the wide ZVS range of the primary MOSFETs and the continuous input current. The operational principles of the proposed converter are analyzed and the advantages are described. The 60W industrial sample of the proposed converter is implemented for digital car audio amplifier to confirm the advantages of the proposed converter. The measured efficiency of the proposed converter is 88.3% at nominal input voltage and it is higher than that of the BHB converter. The proposed converter is expected to be suitable for the high efficiency and low profile on-board DC/DC converter for digital car audio amplifier.

Acknowledgment

This research was supported by university IT research center project.

References

[1] N.-S. Jung, N.-I. Kim; G.-H. Cho, "A new high-efficiency and super-fidelity analog audio amplifier with the aid of digital switching amplifier: class K amplifier," *IEEE PESC 1998*, Vol. 1, pp. 457 – 463. May, 1998.

[2] J. Zeng, J. Ying, Q. Zhang, "A novel DC/DC ZVS converter for battery input application," *IEEE APEC 2002*, Vol. 2, pp. 892 –896, March, 2002.

[3] H. Watanabe, H. Matsuo, "A novel high-efficient DC-DC converter with 1V/20A DC output," *IEEE INTELEC 2002*, pp. 34 –39, Sept.-Oct., 2002.